Far-field Fano resonance in nanoring lattices modeled from extracted, point dipole polarizability

Drew DeJarnette, Phillip Blake, Gregory T. Forcherio, and D. Keith Roper

Citation: Journal of Applied Physics **115**, 024306 (2014); doi: 10.1063/1.4858396
View online: http://dx.doi.org/10.1063/1.4858396
View Table of Contents: http://scitation.aip.org/content/aip/journal/jap/115/2?ver=pdfcov
Published by the AIP Publishing

Far-field Fano resonance in nanoring lattices modeled from extracted, point dipole polarizability

Drew DeJarnette,[1] Phillip Blake,[2] Gregory T. Forcherio,[1] and D. Keith Roper[1,2,a)]
[1]*Microelectronics and Photonics Graduate Program, University of Arkansas, Fayetteville, Arkansas 72701, USA*
[2]*Department of Chemical Engineering, University of Arkansas, Fayetteville, Arkansas 72701, USA*

(Received 4 October 2013; accepted 10 December 2013; published online 10 January 2014)

Coupling and extinction of light among particles representable as point dipoles can be characterized using the coupled dipole approximation (CDA). The analytic form for dipole polarizability of spheroidal particles supports rapid electrodynamic analysis of nanoparticle lattices using CDA. However, computational expense increases for complex shapes with non-analytical polarizabilities which require discrete dipole (DDA) or higher order approximations. This work shows fast CDA analysis of assembled nanorings is possible using a single dipole nanoring polarizability extrapolated from a DDA calculation by summing contributions from individual polarizable volume elements. Plasmon resonance wavelengths of nanorings obtained using extracted polarizabilities blueshift as wall dimensions-to-inner radius aspect ratio increases, consistent with published theory and experiment. Calculated far-field Fano resonance energy maximum and minimum wavelengths were within 1% of full volume element results. Considering polarizability allows a more complete physical picture of predicting plasmon resonance location than metal dielectric alone. This method reduces time required for calculation of diffractive coupling more than 40 000-fold in ordered nanoring systems for 400–1400 nm incident wavelengths. Extension of this technique beyond nanorings is possible for more complex shapes that exhibit dipolar or quadrupole radiation patterns. © *2014 AIP Publishing LLC*.
[http://dx.doi.org/10.1063/1.4858396]

I. INTRODUCTION

Subwavelength, metallic nanostructures are of widespread interest due to their ability to confine and manipulate incident light from collective electron oscillation or plasmons. Wavelength-scale ordering of such nanostructures supports Fano resonances that are observed[1] and predicted[2–4] from coupling between localized plasmon oscillation and coherent scattered light. Optical responses of individual and interacting plasmonic nanoarchitectures have primarily been ascribed to microscopic dielectric functions of bulk metal and its surrounding medium. Associated plasmon resonance has been modulated by tuning the surrounding dielectric, reshaping the structure of the nanoelement[5] or organizing nanoelements into periodic structures to induce near[6] and far-field interactions.[7] Enhanced optical responses have been observed in nanoparticle structures such as spheres, disks, rings, dolman, shells, or disk/ring heterostructures. Such enhancements are reported to increase absorption in the Fano resonance window which allows high-performance and nonlinear optics.[8] However, expensive computational approaches required to predict and optimize optical behavior in metallic nanoarchitectures of increasing complexity often obscure effects of organization, shape, and dielectric functions on spectral features and systems-level outcomes such as sensitivity. Furthermore, design of microscopic arrays of subwavelength nanostructures for predictable control of light in chemical and biological sensors,[9] waveguides,[10] optical resonantors,[11] enhanced terahertz device,[12] and photodetection[13] is slowed by the inability to bridge electrodynamic simulation of nanoscale interactions to geometric optical descriptions of micro-scale systems.

Plasmonic coupling and extinction of incident energy by nanoscale geometries may be expressed constitutively in a particle polarizability to support computational analysis. Polarizabilities for nanorings have been described analytically[14] as well as extracted from numerical finite difference time domain (FDTD)[15] to understand plasmonic behavior in nanostructures. Analytic polarizability results for nanotoroids to date are limited to the non-retarded case, where the nanostructure is much smaller than the incident wavelength. The reported polarizability extraction method requires numeric volume integration of the frequency-dependent charge distribution which was determined using the electric field divergence from Fourier transformed time-dependent fields calculated using FDTD. Polarizability extraction from FDTD has only been applied to near-field, nanostructure interactions using a Fano interference model. Dipole and quadrupole contributions to single particle extinction have also been determined using the discrete dipole approximation (DDA) by calculating the single particle dipole moment and quadrupole tensor.[16] However, this did not include specific single particle polarizability calculations.

Plasmon resonance in a subwavelength, dispersive nanoparticle results from incident irradiation at energies for which specific negative values of the material dielectric arise.[17] Nanoparticle morphology and thus polarizability can

a)Author to whom correspondence should be addressed. Electronic mail: dkroper@uark.edu.

be modulated to shift the frequency-dependent value of dielectric that produces resonance, preserving a time averaged electromagnetic energy inside the particle that is greater than the energy in the medium.[18] For nanorings in the non-retarded case, increasing wall thickness increases particle volume and aspect ratio, which is compensated by a blueshift in plasmon resonance that preserves the greater energy inside the particle.

Polarizability-based simulations of plasmon resonance trends due to particle-particle coupling have primarily been calculated using the DDA and coupled dipole approximation (CDA). In particular, the CDA has been largely used to determine coupling from scattering and absorption of spheroidal particles due to the complexity of calculating polarizabilities for non-spheroidal shapes. Effects of lattice dimensions, particle polarizability, and environmental refractive index have been examined previously for spherical particles.[19] One prior CDA formulation evaluated decomposed eigenmodes in an infinite periodic lattice using Green's function to sum lattice scattering and an independent expression for dipole polarizability.[20] Recent CDA models described nanodisks as spheroids[21,22] and applied CDA results calculated from spheres to describe gap-separated bowtie antenna.[6]

This work extracts a complex-valued polarizability for a defined nanoring geometry from DDA computation for insertion into a computationally inexpensive CDA simulation. This permits rapid calculation of coupling interactions of non-spheroidal nanoparticles and examination of singular influences of polarizability in the occurrence of far-field Fano resonances. Arbitrarily shaped particles that exhibit predominately dipolar and/or quadrupolar radiative patterns are amenable to this approach. Polarizability effects on far-field Fano resonances in square lattices of nanorings are considered due to the increased recent interest in toroidal nanoantennae. This interest results from high tunability of plasmon resonance by modifying ring dimensions. Nanoring interactions were rapidly simulated to predict far-field Fano resonance produced from an infrared grating in a periodic lattice. Fano resonance was shown to interfere with the single nanoring plasmon peak, causing a bifurcation into two distinct spectral peaks: one each from plasmon and Fano resonances. Control of spectral location and bandwidth were attributed directly to periodic arrangement of the nanoring lattice. These results support development of enhancements in plasmonic devices by reducing computational costs to simulate complex shapes, such as nanorings shown here, using a point dipole/quadrupole model. This method reduced computation time by more 40 000-fold for infinite arrays computed using the CDA opposed to the DDA. This work accelerates previous models such as Ref. 20 by allowing complex structures to be modeled in the CDA.

II. METHODS

Consider a square lattice of coupled, subwavelength gold (Au) nanorings with pitch greater than or equal to single particle plasmon wavelength. The CDA computes polarization, P_i, for each ring in proportion to superposed contributions from both the incident electromagnetic field, E_{inc}, and the lattice, E_{dipole}, viz.,

$$P_i = \alpha(E_{inc} + E_{dipole}). \tag{1}$$

Contributions to the electric fields from the point dipoles (E_{dipole}) in the lattice may be calculated using a retarded dipole sum as expressed in Refs. 7, 23, and 24. This work computes polarizability, α, of a single nanoring using a separate DDA simulation. The nanoring was discretized into 10 425 dipoles for the specific case shown in Fig. 2. The aggregate nanoring polarizability was determined by summing the polarizabilities for each discretized unit, using a frequency-dependent dielectric function for Au.[25] Aggregate polarizability for a nanoring of a particular geometry was substituted into the CDA which computes interactions between a finite number of nanorings in a user defined arrangement and a rapid, semi-analytical solution to the coupled dipole approximation (rsa-CDA).[23,24] The CDA is well suited to compute electromagnetic interactions in the far-field when particle separations are greater than the particle dimensions.[7] The rsa-CDA uses array symmetry to describe infinite lattices of point dipoles in order to reduce computational expense and increase finely resolved features compared to the point-by-point computation of infinite lattices. This permits evaluation of Fano resonance features from more than 40 000 arrays, each truncated at 40 000 nanoparticles with any arbitrary inter-particle spacings greater than the single nanoring dimensions, in the time it takes to perform a single DDA simulation.

Effective polarizability tensors for each nanoring geometry were obtained from an approximate discrete dipole solution from DDSCAT 7.3.[26–28] DDSCAT solves Maxwell's equations for an arbitrary target geometry by treating the target as a conglomerate of polarizable dipoles, which result in the absorption and scattering of an electromagnetic wave. The polarizability of each assumed dipolar point was chosen according to a "lattice dispersion relation" for cubic lattices described by Gutkowicz-Krusin *et al.* by using the "GKDLDR" option within DDSCAT.[29] Each nanoring geometry was discretized into the target of constituent cubically arranged dipolar points, as seen in Fig. 2, using a MATLAB script. The effective polarizability, α_{eff}, of this discretized target was calculated as a function of the inter-dipole spacing (d), the complex polarization of the ith dipole per unit volume (P_i), and the incident complex electric field $(E_{inc})_i$ at the ith dipole given by

$$\alpha_{eff} = \sum \frac{d^3 P_i}{(E_{inc})_i}. \tag{2}$$

DDSCAT code was modified to output the real and imaginary components of effective polarizability for a particular nanoring geometry (thickness, height, and inner radius) immersed in a uniform vacuum at individual wavelengths between 400 nm and 1400 nm in 1 nm increments, in addition to producing absorption and scattering spectra. More coarse wavelength discretization and interpolating polarizability values for smaller discretization values in the CDA can

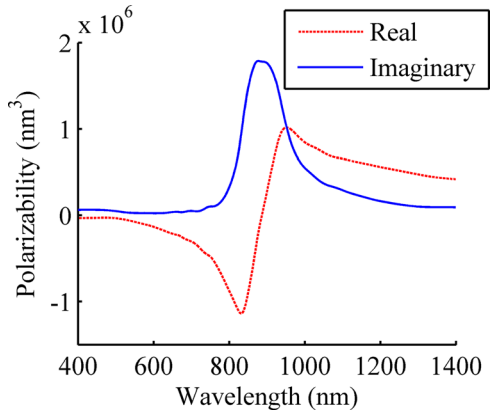

FIG. 1. Real (solid-blue) and imaginary (dotted-red) components of polarizability of a nanoring with inner radius 60 nm, wall thickness 10 nm, height 50 nm calculated using Eq. (2).

further speed computation. Nanorings were simulated by DDA using a constant inter-dipole spacing of 3.33 nm. This resulted in a variation in total number of dipoles (N) between different geometries, which can change spectral peak locations and magnitudes. Nanoring geometries investigated herein had an inner radius of 50, 60, and 75 nm with 10 nm thickness at a height of 50 nm. Polarizability of the 60 nm inner radius ring calculated using Eq. (2) is shown in Fig. 1. Absorption and scattering responses at individual incident wavelengths from isolated gold nanoring immersed in a vacuum environment were evaluated. Detailed comparisons and developments of different reported simulation methods in Refs. 30–32 include DDA, FDTD, boundary element methods (BEM), and finite element methods (FEM) where computed nanostructure spectra were compared and time requirements given for each computational method.

III. RESULTS

Extinction spectra of square lattices of nanorings calculated using the polarizability extraction with the CDA gave spectra with feature maxima and minima within 1% of full numerical DDA simulations. Fig. 2 compares spectra of a single nanoring computed using DDA (black-solid) with comparable arrays of such nanorings evaluated in three ways: (1) a 10×10 array of 60 nm inner radius nanorings spaced at 900 nm array using the CDA (red-dashed); (2) an infinite array spaced at 900 nm using the DDA with periodic boundary conditions (black-dotted); and (3) an infinite array of nanorings spaced at 900 nm calculated via rsa-CDA (magenta-solid). At this spacing, the Fano resonance feature appeared in the window of the single ring localized surface plasmon resonance (LSPR). Each simulation exhibited an extinction minima in the window due to surface lattice resonance from the Rayleigh anomaly located at the lattice constant. The asymmetric, far-field Fano resonance appeared immediately redshifted from the Rayleigh anomaly. While diffractive coupled plasmon resonance in arrays of nanospheres,[4,7] rods,[33,34] and disks[1,35,36] has been previously predicted and measured, far-field Fano resonance of nonspheroidal like nanorings has not been reported.

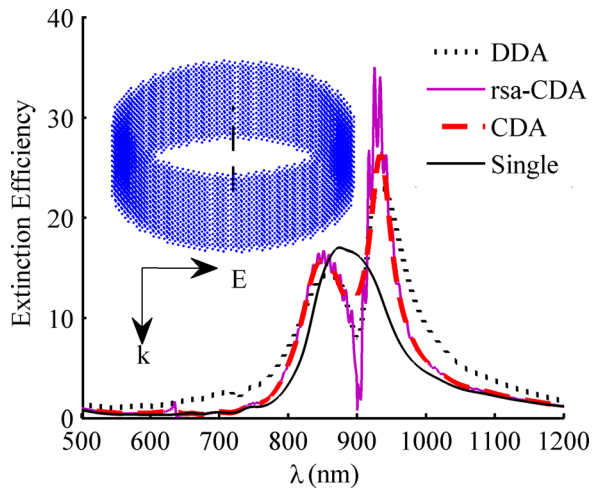

FIG. 2. Comparison of 60 nm inner radius, 10 nm thick, and 50 nm height nanorings in 900 nm spaced square lattices using infinite DDA, finite CDA, and infinite rsa-CDA against the single particle extinction. Polarizability for the rings used in the CDA was extrapolated from DDA simulations for a single ring.

Extinction efficiencies were calculated by dividing the extinction cross section by the cross sectional area of the particle. For the simulated nanorings, to the cross sectional area is 1300π nm^2, equivalent to a 36 nm sphere. Because the CDA simulations overestimated the extinction when using this value, a cross sectional area of 3025π nm^2 was used, which corresponded to a 55 nm radius sphere, to illustrate correspondence between DDA and CDA simulations. Overestimation of extinction is attributed to the point-dipole treatment of the CDA. Extinction is based on the optical theorem, which assumes an incident plane wave. Conversely, DDA calculates extinction based upon the internal electric field at every dipole. It is anticipated that morphology of the structure including interactions and damping between dipoles is not fully taken into account by the polarizability extraction method presented here. Wavelength of the surface lattice resonance resulting from the Rayleigh anomaly was identical for the DDA and rsa-CDA at 900 nm. This spectral dip is a result of Fano resonance and is seen in a variety of system as described by the review in Ref. 2. The finite CDA gave a value 1% lower at 890 nm. This small discrepancy is likely due to the finite nature of the CDA formulation. Wavelengths at which the Fano resonance peaked for DDA, rsa-CDA, and the CDA were 938, 929, and 934 nm, respectively. Corresponding full width at half max (FWHM) values of 55, 38, and 30 nm were obtained.

Interparticle spacings that fall in close proximity to the plasmon wavelength generate Fano resonance where diffractive interference can significantly reduce bandwidth of the plasmon peak. Fig. 2 shows the single nanoring peak narrowing with the FHHM reduced from 126 nm in the single nanoring to 55 nm from the Fano peak corresponding to the plasmon frequency. When the plasmon and inter-particle spacings are farther apart, the plasmon peak broadens and red shifts until it reaches the value of the single particle case (data not shown). This ability to reduce the FWHM could be coupled with far-field Fano resonance for applications where smaller bandwidth is beneficial such as increase sensor performance.[15]

Insertion of DDA-calculated polarizabilities into CDA computation speeds large scale optimization of array parameters. Having computed the polarizability for a particular single ring geometry using the DDA, use of this polarizability in the CDA can generate spectra for arbitrary arrangements of nanorings using the finite CDA and periodic arrangements using the rsa-CDA. Computation times for the finite CDA for arrays of 100 particles require approximately 0.03 h for a wavelength range from 400 to 1400 in 1 nm increments. The rsa-CDA for infinite lattices requires approximately 0.002 h per simulation for the same wavelength range. This is compared to 47.5 h using the DDA for a single nanoring composed of 10 425 dipoles and a required 82.5 h for the infinite array utilizing periodic boundary conditions. All CDA and DDA computations were performed with a 2.40 GHz quad core Intel Xeon with 14 GB memory.

Complex valued polarizabilities extracted from the DDA for a single nanoring were inserted into the finite CDA and rsa-CDA to calculate interactions from periodic arrays. To verify the utility of the single dipole approach, DDA was used to output electric near-field results for a single nanoring with orthogonal excitation polarized along the x-axis. Electric field intensity (E/E_0), shown in Fig. 3, is given in the x-y plane at $z = 0$ for two distinct wavelengths corresponding to the plasmon mode at 855 nm (a), the lattice constant at 900 nm (b), and the far-field Fano resonance at 938 nm (c). These wavelengths were chosen based upon the spectra shown in Fig. 2. Electric field intensity inside the ring was not calculated and finer discretization using 47 500 dipoles with 2 nm dipole spacing for the ring was chosen to achieve convergence of calculated electric fields.[37] Each plot shows electric field intensity corresponding to that of a dipole. Field intensity in all plots was set to 5 to compare dipole strength for both plasmon and associated Fano resonance modes with maxima being 4.6, 3.1, and 7.9 for plasmon (a), lattice constant (b), and Fano (c) resonances indicating a 71% enhancement in the electric field strength at the Fano resonance over the plasmon peak for this specific array.

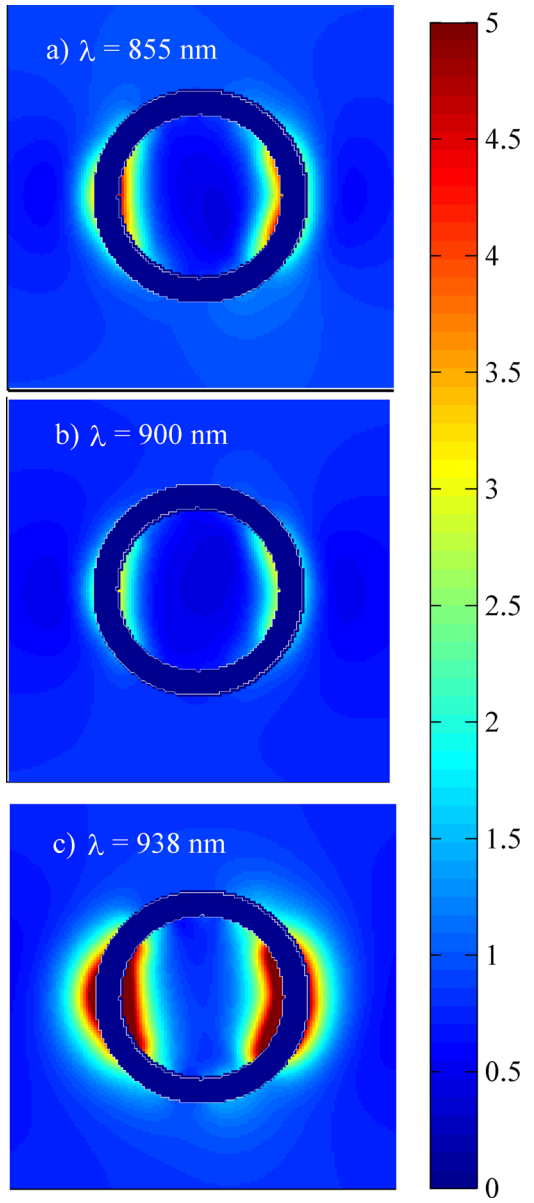

FIG. 3. Electric field intensity plots of simulated nanorings calculated using the DDA with 47 500 dipoles at wavelengths of 855 (a), 900 (b), and 938 nm (c) corresponding to plasmon, lattice constant, and Fano resonance, respectively.

IV. COMPARISON TO SINGLE NANORINGS IN LITERATURE

Single nanorings simulated by inserting a DDA-computed polarizability into CDA computation exhibit plasmon spectral shifts comparable to previously reported single nanorings over a broad range of nanoring aspect ratios. Table I shows trends of blueshifts in plasmon resonance with increasing aspect ratio of the ring. For nanorings, the aspect ratio was determined by dividing the diagonal length of the wall (d) by the inner radius (r_{in}) labeled in Fig. 4 inset while the nanotori aspect ratios are the wall diameter divided by the inner radius. Inner radii from 46 to 75 (21 to 77.5) nm with a wall thickness range of 9 to 50 (12 to 25) nm are shown for rings (tori). Reported values were selected due to their dimensional similarity to the simulations in this work. Even for the small size range in the table, the LSPR peak wavelength ranges from ~800 to 1360 nm. This wide range indicates that nanoring plasmons and corresponding spectral features are very sensitive to small changes in their dimensions.

Nanoring spectra summarized in Table I compared spectral features from both experimental and computational sources—except those of Refs. 15, 38, and 39 which include only computation. Aizpurua *et al.* reported a wavelength change of −190 nm using the BEM when ring aspect ratio was increased by a relative 2.6%.[5] In contrast, a relative increase of 7.7% in aspect ratio corresponded to a resonance change of 126 nm comparing the polarizability extraction from the DDA reported here simulation (2) in Table I to values reported using BEM by Aizpurua *et al.*[5] However, the apparent redshift for increasing aspect ratio in the latter case is between two different computational methods. Absolute values of plasmon resonance from the BEM in Ref. 5 are larger than FDTD and DDA values owing to inclusion of a substrate in the BEM. Trends and quantitative plasmon resonance location from simulations in this work correspond

TABLE I. Comparison of simulated, single nanoring plasmon peak from published data.

r_{in} (nm)	t (nm)	h (nm)	d (nm)	AR d/r_{in}	LSPR (nm)	Simulation method
Ring						
75	25	50	55.9	0.743	950	FDTD[15]
63	24	24	33.9	0.538	1015	FDTD[41]
50	50	50	70.7	1.41	775	FDTD[41]
50	15	62	63.7	1.27	798[a]	FDTD[40]
46	14	40	42.4	0.921	1000	BEM[5]
50	10	40	41.2	0.824	1170	BEM[5]
51	9	40	41.0	0.804	1360	BEM[5]
48.5	11.5	60	61.1	1.26	1030[b]	FEM[42]
50	10	50	51.0	1.02	790	DDA (1)
60	10	50	51.0	0.85	874	DDA (2)
75	10	50	51.0	0.68	950	DDA (3)
Torus						
21	…	…	21	1	625	MOM[38]
27	…	…	15	0.56	833	Analytic[14]
30	…	…	12	0.4	910	Analytic[14]
77.5	…	…	25	0.32	1200	BEM[39]

[a]Nanoring height not given in publication. Data point not shown in Fig. 4 due to uncertainty in value ranging from 30 to 92 nm.
[b]Plasmon value given in water RI.

well to FDTD and BEM, when inclusion of a substrate for the BEM is considered. Results from Table I are shown in Fig. 4 for each of the computation methods used to simulate both nanorings and nanotori.

Nanoring plasmon resonance generally blueshifts with increasing aspect ratio as Fig. 4 illustrates. Blueshifting trends in nanorings were explained by Aizpurua *et al.* using a Drude-based model for a slab rolled into a ring.[5] It was shown that for the long wavelength approximation, blueshifts of plasmon resonance corresponded to decreases in the expression $\exp(-nt/r)$, where n is the mode ($n=1$ for dipole), t is the thickness, and r is the inner radius. For nanotori, the analytic polarizability is expressed in toroidal coordinates and shows that plasmon resonance location is dependent on the surface of the torus, q_1^0, defined by $d/r_{in} = 2\cosh(q_1^0 - 1)$ which also indicates that increasing aspect ratio results in a blueshifted plasmon resonance.[14] The exact dependence of plasmon resonance on aspect ratio of nanotori is expressed as products and sums of associated Legendre functions and is not given here.

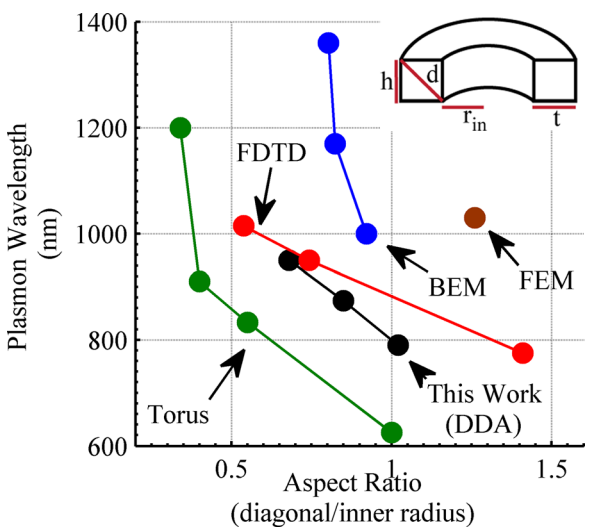

FIG. 4. Trends of plasmon peak wavelength for increasing aspect ratio of nanorings calculated the boundary element method (blue), finite difference time domain (red), finite element reported in a water background (brown), and discrete dipole approximation from this work (black). Also shown are trends for nanotori using a variety of methods (green). Inset is a schematic showing a nanoring with inner radius (r_{in}), thickness (t), height (h), and diagonal (d) labeled.

These expressions, together with the spectral shifts illustrated in Fig. 4, indicate that while the negative values of the real component of metal dielectric functions indicates plasmonic behavior, the exact energies and red/blue shifts of corresponding spectral features arise from geometric consideration. Polarizability combines effects of dielectric and particle morphology in describing spectral occurrence of particle plasmons. Inserting a model of polarizability into a description of retarded fields allows effects of metamaterial arrangement on spectral behavior to be explained. As a result, models such as polarizability and Drude's theory of metals allow plasmonic behavior to be predicted and understood on a physical level.

Spectral shifting of nanoring plasmons has been attributed to coupling of positive and negative electromagnetic modes between the inner and outer nanoring surface, resulting in a mode splitting polarization scheme.[43] Each mode is split into symmetric with positive and negative charge at opposite ends of the ring and anti-symmetric where each side contains both positive and negative charge on the inner and outer walls (not shown). As the thickness of a nanoring increases, the symmetric mode blueshifts and both modes converge to that of a single disk. Additionally, as ring thickness decreases and approaches the mean free path of coherently oscillating electrons at the LSPR frequency (~10 nm in gold[32]),[44] the probability of electron collisions within the ring increases. When the dimensions are less than this bulk mean free path, electron collisions with the surface of the NP reduce the mean free path which blue shifts and broadens the LSPR wavelength.[45] However, modeling effects of nonlocality of the dielectric function due to nanoring dimensions on the order of the mean free path is not readily available and thus not presented in this work. Even so, simulated trends presented in this work as shown in Table I and Fig. 4 correspond well with trends expected from existing explanations based upon polarizability and Drude models.

Future work using this method will extend the implementation to include quadrupole interactions as well. The CDA can accurately compute far-field spectra for ordered shapes that possess a quadrupole mode in addition to the dipole mode using an extension to the dipole polarizability[23] or separate quadrupole scattering calculations.[46] As a result, complex nanostructures with in-plane dipole and quadrupole far-field profiles can utilize polarizabilities extracted from DDA computation by fitting individual dipole and quadrupole Lorentzian peaks to the spectra generated using Eq. (2). Interactions from extracted quadrupole and dipole polarizabilities can be determined by the CDA to examine effects of nanoparticle separation and arrangement on the overall extinction spectra.

V. CONCLUSIONS

This work introduces a method to enhance analysis of resonance coupling in arrays of complex nanoparticle shapes by extracting polarizability from a DDA by summing individual dipole polarizabilities with a discretized volume. Electromagnetic interactions between arrayed nanostructures that possess electric field distributions which can be represented as a point dipole or quadrupole can be rapidly calculated. This method was illustrated by extracting the polarizability for a single nanoring from the DDA and employing it in the CDA to simulate an array of interacting nanorings. Blueshifts in single ring plasmon resonance location with increasing aspect ratio was found to be consistent with current experimental and computational results. Changes in far-field Fano resonance features due to interparticle coupling with respect to relative placement of nanoparticles in a lattice were examined using a constitutive polarizability. Simulated nanoring lattices were shown to exhibit less than 1% error in Fano resonance location between full discrete dipole approximation and the more rapid coupled dipole approximation with a 40 000-fold computation time reduction per array over the spectral range of 400–1400 nm.

ACKNOWLEDGMENTS

This work was supported in part by NSF CMMI-0909749, NSF CBET 1134222, NSF ECCS-1006927, the Walton Family Charitable Support Foundation, and the University of Arkansas Foundation. Any opinions, findings, and conclusions or recommendations expressed in this material are those of the authors and do not necessarily reflect the views of the National Science Foundation. D. DeJarnette performed CDA simulations and prepared data and text for the manuscript. P. Blake performed DDA simulations and prepared preliminary text. G. Forcherio performed DDA simulations and aided in text revision. D. K. Roper directed the work and prepared and organized the final text.

[1]Y. Chu, E. Schonbrun, T. Yang, and K. B. Crozier, Appl. Phys. Lett. **93**, 181108 (2008).
[2]Y. Francescato, V. Giannini, and S. A. Maier, ACS Nano **6**, 1830 (2012).
[3]V. Giannini, Y. Francescato, H. Amrania, C. C. Phillips, and S. A. Maier, Nano Lett. **11**, 2835 (2011).
[4]D. DeJarnette, J. Norman, and D. K. Roper, Appl. Phys. Lett. **101**, 183104 (2012).
[5]J. Aizpurua, P. Hanarp, D. Sutherland, M. Käll, G. Bryant, and F. García de Abajo, Phys. Rev. Lett. **90**, 057401 (2003).
[6]D. P. Fromm, A. Sundaramurthy, P. J. Schuck, G. Kino, and W. E. Moerner, Nano Lett. **4**, 957 (2004).
[7]L. Zhao, K. L. Kelly, and G. C. Schatz, J. Phys. Chem. B **107**, 7343 (2003).
[8]Y. Zhang, F. Wen, Y.-R. Zhen, P. Nordlander, and N. J. Halas, Proc. Natl. Acad. Sci. U.S.A. **110**, 9215 (2013).
[9]S.-H. Wu, S.-Y. Hsieh, K.-L. Lee, R.-H. Weng, A. Chiou, and P.-K. Wei, Appl. Phys. Lett. **103**, 133702 (2013).
[10]T.-T. Le and L. Cahill, Opt. Commun. **301–302**, 100 (2013).
[11]K. X. Wang, Z. Yu, S. Sandhu, and S. Fan, Opt. Lett. **38**, 100 (2013).
[12]J. Li and S. Zouhdi, IEEE Photonics Technol. Lett. **24**, 625 (2012).
[13]Z. Fang, Z. Liu, Y. Wang, P. M. Ajayan, P. Nordlander, and N. J. Halas, Nano Lett. **12**, 3808 (2012).
[14]A. Mary, D. Koller, A. Hohenau, J. Krenn, A. Bouhelier, and A. Dereux, Phys. Rev. B **76**, 245422 (2007).
[15]F. Hao, P. Nordlander, Y. Sonnefraud, P. Van Dorpe, and S. A. Maier, ACS Nano **3**, 643 (2009).
[16]F. Zhou, Z.-Y. Li, Y. Liu, and Y. Xia, J. Phys. Chem. C **112**, 20233 (2008).
[17]I. Mayergoyz, D. Fredkin, and Z. Zhang, Phys. Rev. B **72**, 155412 (2005).
[18]F. Wang and Y. Shen, Phys. Rev. Lett. **97**, 206806 (2006).
[19]D. DeJarnette, J. Norman, and D. K. Roper, Photonics Res. **2**, 15 (2014).
[20]Y.-R. Zhen, K. Fung, and C. Chan, Phys. Rev. B **78**, 035419 (2008).
[21]S. H. Alavi Lavasani and T. Pakizeh, J. Opt. Soc. Am. B **29**, 1361 (2012).
[22]T. Pakizeh and M. Käll, Nano Lett. **9**, 2343 (2009).
[23]D. DeJarnette, D. K. Roper, and B. Harbin, J. Opt. Soc. Am. B **29**, 88 (2012).
[24]D. K. Roper, W. Ahn, B. Taylor, and A. G. Dall'Asen, IEEE Sens. J. **10**, 531 (2010).
[25]P. Johnson and R. Christy, Phys. Rev. B **6**, 4370 (1972).
[26]B. T. Draine and P. J. Flatau, J. Opt. Soc. Am. A **11**, 1491 (1994).
[27]B. T. Draine and P. J. Flatau, J. Opt. Soc. Am. A Opt. Image Sci. Vis. **25**, 2693 (2008).
[28]B. Draine and P. Flatau, "User guide for the discrete dipole approximation code DDSCAT 7.3," preprint arXiv:1305.6497 (2013).
[29]D. Gutkowicz-Krusin and B. Draine, "Propagation of electromagnetic waves on a rectangular lattice of polarizable points," preprint arXiv:Astro-Ph/0403082 1 (2004).
[30]W. L. Barnes, J. Opt. A, Pure Appl. Opt. **11**, 114002 (2009).
[31]J. Zhao, A. O. Pinchuk, J. M. McMahon, S. Li, L. K. Ausman, A. L. Atkinson, and G. C. Schatz, Acc. Chem. Res. **41**, 1710 (2008).
[32]V. Myroshnychenko, J. Rodríguez-Fernández, I. Pastoriza-Santos, A. M. Funston, C. Novo, P. Mulvaney, L. M. Liz-Marzán, and F. J. G. de Abajo, Chem. Soc. Rev. **37**, 1792 (2008).
[33]N. Félidj, G. Laurent, J. Aubard, G. Lévi, A. Hohenau, J. R. Krenn, and F. R. Aussenegg, J. Chem. Phys. **123**, 221103 (2005).
[34]D. Weber, P. Albella, P. Alonso-González, F. Neubrech, H. Gui, T. Nagao, R. Hillenbrand, J. Aizpurua, and A. Pucci, Opt. Express **19**, 15047 (2011).
[35]V. Kravets, F. Schedin, and A. Grigorenko, Phys. Rev. Lett. **101**, 087403 (2008).
[36]B. Auguié and W. L. Barnes, Opt. Lett. **34**, 401 (2009).
[37]E. Hao and G. C. Schatz, J. Chem. Phys. **120**, 357 (2004).
[38]N. Burford and M. El-Shenawee, Appl. Comput. Electromagn. Soc. J. **28**, 359 (2013).
[39]T. V. Teperik and A. Degiron, Phys. Rev. B **83**, 245408 (2011).
[40]C. Huang, J. Ye, S. Wang, T. Stakenborg, and L. Lagae, Appl. Phys. Lett. **100**, 173114 (2012).
[41]F. Hao, E. M. Larsson, T. A. Ali, D. S. Sutherland, and P. Nordlander, Chem. Phys. Lett. **458**, 262 (2008).
[42]H.-Y. Tseng, C.-K. Lee, S.-Y. Wu, T.-T. Chi, K.-M. Yang, J.-Y. Wang, Y.-W. Kiang, C. C. Yang, M.-T. Tsai, Y.-C. Wu, H.-Y. E. Chou, and C.-P. Chiang, Nanotechnology **21**, 295102 (2010).
[43]J. Aizpurua, L. Blanco, P. Hanarp, D. S. Sutherland, M. Käll, G. W. Bryant, and F. J. G. de Abajo, J. Quant. Spectrosc. Radiat. Transf. **89**, 11 (2004).
[44]S. Link, C. Burda, Z. L. Wang, and M. A. El-Sayed, J. Chem. Phys. **111**, 1255 (1999).
[45]J. Z. Zang, *Optical Properties and Spectroscopy of Nanomaterials* (World Scientific, London, 2009).
[46]A. B. Evlyukhin, C. Reinhardt, U. Zywietz, and B. N. Chichkov, Phys. Rev. B **85**, 245411 (2012).